The influence of internal model variability in GEOS-5 on interhemispheric CO_2 exchange

Melissa Allen,[1] David Erickson,[2] Wesley Kendall,[3] Joshua Fu,[1] Lesley Ott,[4] and Steven Pawson[4]

Received 26 October 2011; revised 15 March 2012; accepted 13 April 2012; published 19 May 2012.

[1] An ensemble of eight atmospheric CO_2 simulations was completed employing the National Aeronautics and Space Administration (NASA) Goddard Earth Observation System, Version 5 (GEOS-5) for the years 2000–2001, each with initial meteorological conditions corresponding to different days in January 2000 to examine internal model variability. Globally, the model runs show similar concentrations of CO_2 for the two years, but in regions of high CO_2 concentrations due to fossil fuel emissions, large differences among different model simulations appear. The phasing and amplitude of the CO_2 cycle at Northern Hemisphere locations in all of the ensemble members is similar to that of surface observations. In several southern hemisphere locations, however, some of the GEOS-5 model CO_2 cycles are out of phase by as much as four months, and large variations occur between the ensemble members. This result indicates that there is large sensitivity to transport in these regions. The differences vary by latitude—the most extreme differences in the Tropics and the least at the South Pole. Examples of these differences among the ensemble members with regard to CO_2 uptake and respiration of the terrestrial biosphere and CO_2 emissions due to fossil fuel emissions are shown at Cape Grim, Tasmania. Integration-based flow analysis of the atmospheric circulation in the model runs shows widely varying paths of flow into the Tasmania region among the models including sources from North America, South America, South Africa, South Asia and Indonesia. These results suggest that interhemispheric transport can be strongly influenced by internal model variability.

Citation: Allen, M., D. Erickson, W. Kendall, J. Fu, L. Ott, and S. Pawson (2012), The influence of internal model variability in GEOS-5 on interhemispheric CO_2 exchange, *J. Geophys. Res.*, *117*, D10107, doi:10.1029/2011JD017059.

1. Introduction

[2] Internal model variability in chemical transport is an important consideration for evaluating atmospheric distributions of carbon dioxide (CO_2). Time-dependent transport patterns, for example, especially between the Northern and the Southern Hemispheres, affect natural internal model variability significantly. For instance, variations in the efficiency of interhemispheric exchange were seen among a variety of global models in the TransCom experiments of *Baker et al.* [2006], *Patra et al.* [2006], *Gurney et al.* [2005], and *Law et al.* [1996, 2003]. Although great strides in model capability have been made in global and regional CO_2 flux estimates, areas of regional sensitivity continue to exist in global model transport representation of these estimates. While GEOS-5 can produce good agreement for approximations of observed CO_2 fluxes at nearly all Northern Hemisphere sites, estimations for Southern Hemisphere locations are less well captured by the model suggesting that further examination of the underlying transport processes are needed.

[3] CO_2 fluxes are influenced by both ocean and land sources and sinks including land sources defined by photosynthesis and respiration in the terrestrial biosphere, fossil fuel emissions and biomass burning. Gradients in atmospheric CO_2 concentration reflect these various earth surface sources and sinks, which (with the exception of biomass burning) are distributed widely over continents and oceans and vary in time and space [*Heimann and Keeling*, 1986]. Historical observations made at Mauna Loa, Hawaii, along with those made since at worldwide stations, indicate that patterns in atmospheric CO_2 distributions have changed nonlinearly with time over the last 10–100 years [*Keeling et al.*, 1976].

[1]Department of Civil and Environmental Engineering, University of Tennessee, Knoxville, Tennessee, USA.
[2]Computational Earth Science Group, Computer Science and Mathematics Division, Oak Ridge National Laboratory, Oak Ridge, Tennessee, USA.
[3]Department of Computer Science, University of Tennessee, Knoxville, Tennessee, USA.
[4]NASA Goddard Space Flight Center, Greenbelt, Maryland, USA.

Corresponding author: M. R. Allen, Department of Civil and Environmental Engineering, University of Tennessee, 59 Perkins Hall, Knoxville, TN 37996-2010, USA. (mallen24@utk.edu)

0148-0227/12/2011JD017059

[4] Transport of species is affected by vertical and horizontal wind patterns along with subgrid processes such as diffusion due to turbulence and cloud mass fluxes. For example, *Law et al.* [1996] found that the efficiency of surface interhemispheric exchange among 12 different three-dimensional atmospheric transport models showed variations in both vertical and horizontal transport. *Erickson et al.* [2008], in estimating seasonal CO_2 cycles from monthly estimates, showed that in midlatitudes, near sources of CO_2 due to anthropogenic emissions, synoptic scale atmospheric circulation had a large effect on the cycle during winter, and that subgrid processes such as boundary layer venting and diurnal rectifier effects influenced summer results more significantly.

[5] We examine eight different GEOS-5 model simulations of CO_2 seasonal cycles in both hemispheres given different initial meteorological conditions, and compare them with observations collected primarily from the National Oceanic and Atmospheric Administration Earth System Research Laboratory (NOAA-ESRL), the Australian Commonwealth Scientific and Industrial Research Organization (CSIRO), Environment Canada (EC), and other agencies by the CarbonTracker Global Modeling Division [*Peters et al.*, 2007]. We then describe some of the possible explanations for differences among the CO_2 seasonal cycles due to regional and interhemispheric flow development in the model.

[6] We present first a description of the GEOS-5 model and the simulations, and the observation data archived by CarbonTracker to which they are compared. Second, we describe the methods of analysis; and finally, we discuss results and conclusions.

2. Methods

2.1. GEOS-5 Model Simulations

[7] The General Circulation Model (GCM) used to simulate variations in CO_2 distribution and transport due to differences in initial meteorological conditions was that of the National Aeronautics and Space Administration's (NASA) Goddard Earth Observation System, Version 5.1.0 (GEOS-5), [*Rienecker et al.*, 2008]. This model uses a flux-form semi-Lagrangian finite-volume dynamical core with floating vertical coordinate developed by Lin and Rood [*Lin*, 2004], which computes the dynamical tendencies of vorticity, divergence, surface pressure and a variety of selected trace constituents. Convective mass fluxes are estimates made by the Relaxed Arakawa-Schubert (RAS) convective parameterization [*Moorthi and Suarez*, 1992]. Shortwave radiation in the model is that of *Chou and Suarez* [1999]. Longwave radiation is documented by *Chou et al.* [2001]. For atmospheric boundary layer turbulent mixing, two schemes are used. *Louis et al.* [1982] is used in stable situations with no or weakly cooling planetary boundary layer (PBL) cloud, while *Lock et al.* [2000] is used for unstable or cloud topped PBLs. Free atmospheric turbulent diffusivities are based on the gradient Richardson number [*Rienecker et al.*, 2008; *Ott et al.*, 2011].

[8] The spatial resolution of the model is a 1-degree $\times$ 1.25-degree latitude-longitude grid with 72 vertical pressure layers that transition from terrain-following near the surface to pure pressure levels above 180 hPa. The top vertical boundary is at 0.01 hPa (near 80 km). At the ocean surface, temperature and sea ice distributions are specified using a global data set.

[9] An eight-member ensemble of free-running model simulations, each initialized with meteorology from different days in January 2000 (e.g., January 1, 3, 5, 7, 9, 11, 13, 15) was performed in order to examine the effect of internal model variability on simulated trace gas distributions. Though initial meteorology differed among ensemble members, all were started with the same set of CO_2 fields. The model CO_2 fields were spun-up for four years prior to the beginning of the ensemble calculations using CO_2 fluxes described in *Kawa et al.* [2004] which is closely based on the TransCom 3 protocol [*Gurney et al.*, 2002]. The ensemble formulation has been previously used in GEOS-5 CO simulations by *Ott et al.* [2010] to investigate the dynamical impacts of biomass burning aerosols. For the two-year ensemble simulations in this study, CO_2 emissions are taken from the TRANSCOM Continuous experiment [*Law et al.*, 2008]. Annual CO_2 ecosystem productivity for the years 2002–2003 in this configuration is from an annually balanced terrestrial biosphere based on computations of net primary productivity from the Carnegie-Ames-Stanford Approach (CASA) biogeochemical model [*Randerson et al.*, 1997]. The values are distributed monthly in each of the eight model runs. Fossil fuel emission estimates are from the EDGAR version 3.2 [*Olivier and Berdowski*, 2001] 1990 spatial distribution scaled to 1998 country-level totals. CO_2 ocean exchange is from 4 $\times$ 5 degree monthly mean CO_2 fluxes derived from sea-surface pCO_2 measurements [*Takahashi et al.*, 1999]. In addition to the standard TRANSCOM protocol of fluxes, carbon emissions from biomass burning are courtesy of the Global Fire Emissions Database version 2 (GFEDv2) [*Randerson et al., 2007*; *van der Werf et al.*, 2006]. Output from the model was generated daily; then daily values were averaged for each month.

2.2. CarbonTracker

[10] The observation data sets used for model comparison are those available from CarbonTracker. These data comprise the measurements of CO_2 mole fraction by the National Oceanic and Atmospheric Administration (NOAA) Earth System Research Laboratory (ESRL) and partner laboratories [*Peters et al.*, 2007]. Samples are collected at surface sites in the NOAA ESRL Cooperative Global Air Sampling Network, the CSIRO Air Sampling Network, Environment Canada, and at other agencies, except those flagged for analysis or sampling problems, or those thought to be influenced by local sources [*Tans et al.*, 1989; *Conway et al.*, 1994]. Sites for which data are available vary each week depending on successful sampling and analysis, and each site's sampling frequency.

[11] For most of the CarbonTracker quasi-continuous sampling sites, an afternoon daytime average mole fraction for each day from the time series is constructed. CarbonTracker samples used for this study are monthly averages of the available data points for each observation location and are those that reported from 2–10 data points per month during the years 2000–2001 (except for Easter Island, for which February and March of 2001 consist of a single data point each).

[12] For both the CarbonTracker archived data and the model runs, time series of average total CO_2 concentrations were generated. The annual cycle signal for these time series was then baseline-subtracted using a forward-differencing Fast Fourier Transform (FFT). A low-pass filter was applied to the data to remove components with a period of less than 4 months. The seasonal amplitude for total atmospheric CO_2 concentrations (and for each component of that total at Cape Grim) was calculated from the difference of simulated annual maximum and minimum values of the total (or individual component) at each specified location.

2.3. Calculations of Interhemispheric Transport Time

[13] Interhemispheric Transport time was calculated using the system of equations given for the box model by *Bowman and Cohen* [1997] under the assumption that the difference in average annual CO_2 in each hemisphere is due to a constant average Northern Hemisphere source from 2000 to 2001:

$$\chi_s(\mathrm{t}) = \frac{1}{2}\left[\left(\chi_N^0 - \frac{S_N}{2\mathrm{r}}\right) + S_N\mathrm{t}\right]$$

$$\chi_N(\mathrm{t}) = \frac{1}{2}\left[\left(\chi_N^0 - \frac{S_N}{2\mathrm{r}}\right) + S_N\mathrm{t}\right]$$

χ(t) = the concentration of CO_2 at time t in a given hemisphere; χ_N^0 = initial Northern Hemisphere concentration; r is the mass flux from the Northern to the Southern hemisphere as a fraction of the initial mass; and S_N is the quantity of the Northern Hemisphere source. In these equations, it can be seen that the difference in concentration between the hemispheres depends on the source strength, but the lag depends only on the interhemispheric mass exchange rate. For our purposes, these equations were rearranged:

$$S_N = \frac{2\chi_N(1) - \chi_N^0}{\frac{1}{2\mathrm{r}} + 1} \tag{1}$$

$$\tau = \frac{2\Delta - \chi_N^0 + \frac{S_N}{2\mathrm{r}}}{S_N} \tag{2}$$

with τ = interhemispheric transport time in units of years, Δ = the change in average CO_2 concentration in the southern hemisphere from 2000 to 2001, and concentration values in units of mol/mol. In our calculations, χ_N^0 is set equal to the average Northern Hemisphere CO_2 concentration in 2000 and $\chi_N(1)$ is the average Northern Hemisphere CO_2 concentration in 2001. r was computed as the percent increase in the annual average Northern Hemisphere CO_2 from 2000 to 2001.

2.4. Integration-Based Flow Analysis

[14] The inverse analysis of flow into Cape Grim was accomplished with integration-based flow analysis techniques [*Kendall et al.*, 2011]. Integration-based flow analysis involves dropping imaginary massless particles into the flow field and then integrating the particle flow based on the velocities at each spatiotemporal point. The integration produces lines that are tangent to the flow field (i.e., field lines). Steady state field lines are the solution to the ordinary differential equation:

$$\frac{d\boldsymbol{x}}{ds} = \boldsymbol{v}(\boldsymbol{x}(s));\ \boldsymbol{x}(0) = (x0, y0, z0) \tag{3}$$

where **x**(s) is a 3D position in space (x, y, z) as a function of s, the parameterized distance along the streamline, and **v** is the steady state velocity contained in the time-independent data set. Time-varying field lines utilize a 4D position in space. The equation is solved using a custom fourth-order Runge-Kutta integration method that takes into account the time-varying hybrid-sigma vertical pressure coordinate (in Pascals per second) and its relationship to the curvilinear structure of the latitude-longitude grid. Subgrid transport processes such as turbulence and cloud mass fluxes are not considered in this idealized flow regime. Additionally, although there is naturally some small numerical error in the integration, the Runge-Kutta method employed uses a trial step at the midpoint to cancel out lower-order error terms, and it results in a practical approximation.

3. Results and Discussion

3.1. Initial Simulation Deviations

[15] A plot of the initial CO_2 fossil fuel concentrations for January 2000 is shown in Figure 1. All eight model simulations also show similar source regions (northeastern U.S., western Europe, eastern Asia) with values ranging from 22.5 to 50 ppm. Spatial differences in concentration represent differences in the resulting average January values due to the diverse initial meteorological conditions among the simulations.

[16] In the *Law et al.* [1996] study, differences of as much as 3 ppm in zonal mean surface concentrations of CO_2 due to fossil fuel emissions were noted among the 12 models. Additionally, the mean meridional gradient at the surface varied among models varied by a factor of two. Our results show that maximum regional differences in fossil fuel CO_2 concentrations in eight simulations by the same model differ by a factor of 3. Figures 2 and 3 depict global values for the deviations from the ensemble mean CO_2 from fossil fuel in parts-per-million for the first month of the simulation (January, 2000), and for the last month (December 2001), respectively. A quantitative description of the percent deviations (shown as fractional amounts) can be found in Table 1. The largest maximum deviation from the mean for January, 2000 (+21%) occurs in simulation P04 in the region of Germany/Poland, and the smallest (7%) in P06—a discrepancy of a factor of 3. In December 2001, the maximum deviation (+22.5%) occurs at the same location in simulation P06, in which the region showed a negative deviation in January 2000. The smallest maximum deviation for this month (7%) is also approximately 1/3 of the largest. Mean deviation from the mean for all simulations, while low (0.005% to 0.26%), and somewhat variable (least and greatest differ by two orders of magnitude in January 2000 and one order of magnitude in December 2001), nevertheless persists from the first month of the run until the last.

[17] In their CO_2 observational network *Tans et al.* [1989] discovered that regionally significant CO_2 sources and sinks are needed to maintain small but persistent spatial gradients,

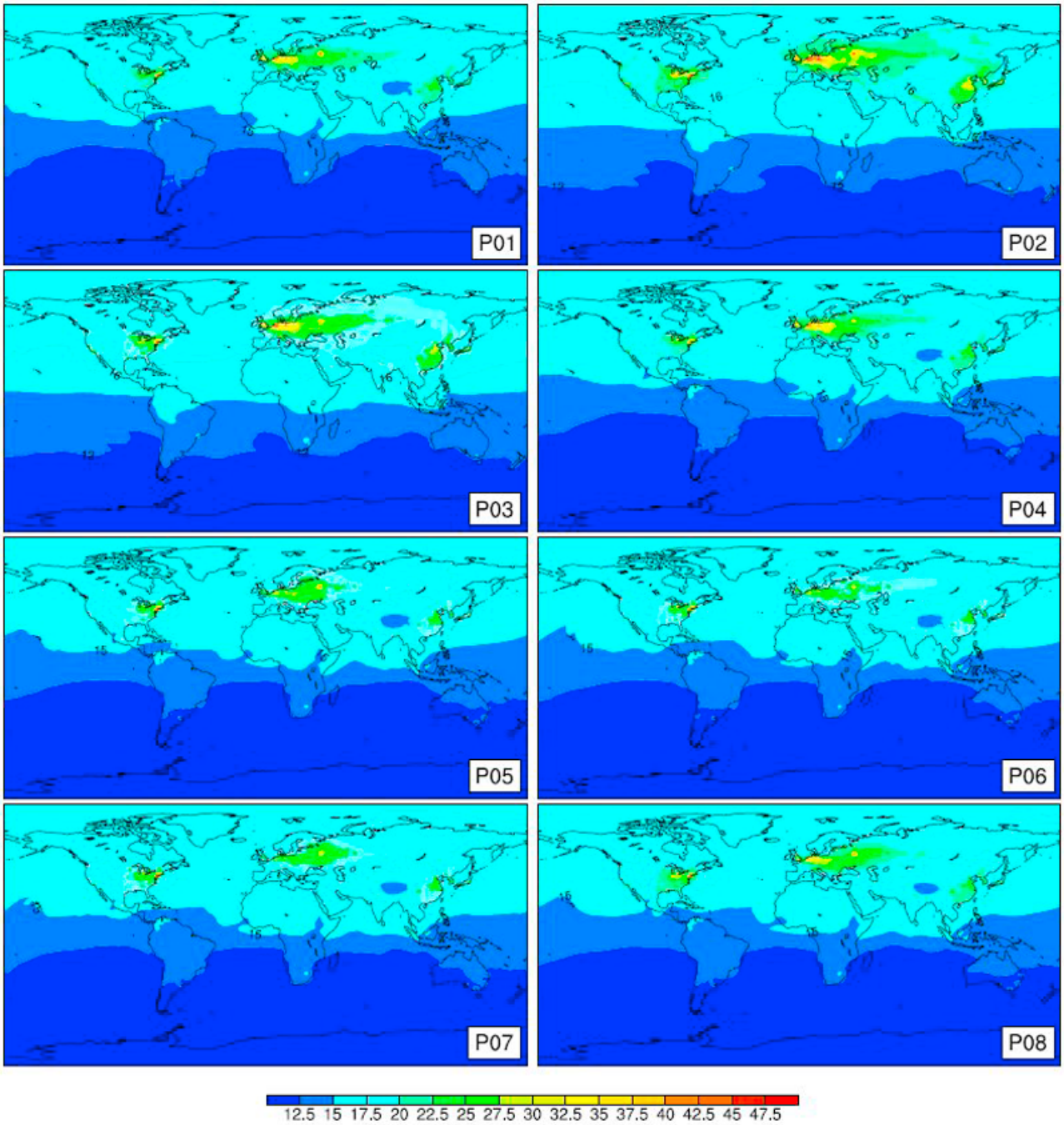

Figure 1. January 2000 lowest atmospheric layer concentrations of CO_2 from fossil fuel in parts per million for the eight model simulations. Spatial differences in concentration represent differences in the resulting average January values due to the diverse initial meteorological conditions among the simulations.

given that atmospheric circulation and mixing are constantly working to homogenize the atmosphere; and that while measurement sites closer to source regions are needed to better determine the effect of sources on the global carbon budget, such measurements do introduce a bias effect. For example, if transport is less vigorous during the season when a surface region is a source rather than when it is a sink, a positive net annual concentration anomaly will result. Nevertheless, it is important to include measurements in regions of sources and sinks, as they will become helpful for monitoring CO_2 emissions more so than the measurements in more stable regions which give information primarily about trends of the background state. These measurements will need to be accounted for in innovative ways, however, in order to increase both observational and model accuracy.

[18] Internal model variability of transport can also affect the flow of air masses differently in regions of sources and sinks to atmospheric CO_2. Even with specified emissions and uptake, there are some regions in which atmospheric CO_2 distribution is strongly affected by transport patterns.

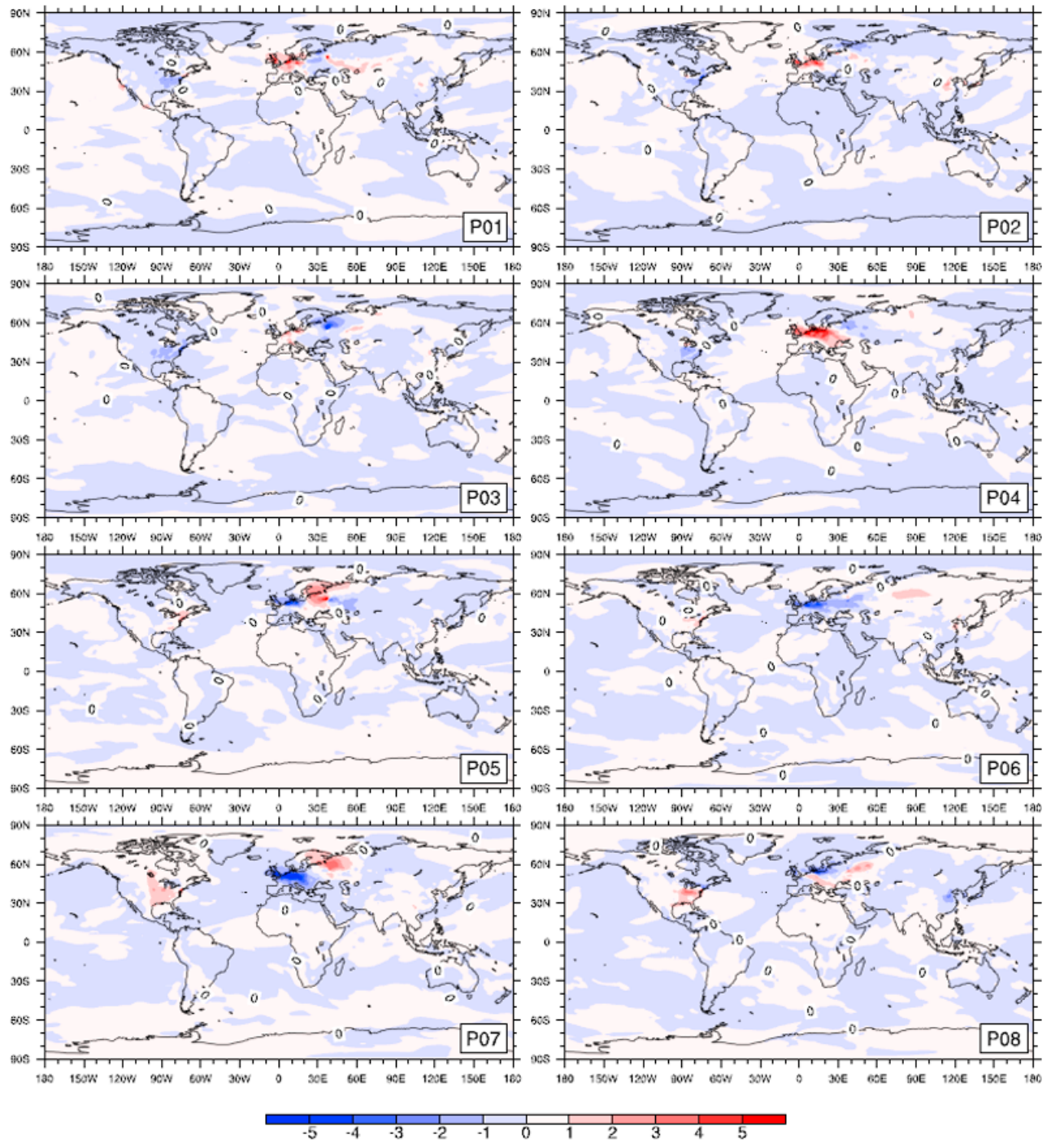

Figure 2. January, 2000, CO_2 from fossil fuel (parts per million): global values for deviations from the eight-ensemble mean. Maximum deviations occur at the dark blue (up to −5 ppm) and dark red (up to +5 ppm) locations.

3.2. CO_2 Cycle Phasing and Amplitude

[19] The uptake and release of atmospheric CO_2 with various surface carbon reservoirs imparts a strong signal on observed atmospheric CO_2 concentrations on time scales ranging from days to years [*Erickson et al.*, 1996]. It is known that the overall seasonal cycle of all sources and sinks is dominated by variation in atmosphere-terrestrial biosphere CO_2 exchange [*Heimann and Keeling*, 1986; *Erickson et al.*, 1996], but ongoing studies evidence the continually emerging fingerprint of fossil fuel emissions as well on both global and regional cycles [*Keeling et al.*, 1989; *Gurney et al.*, 2005; *Erickson et al.*, 2008].

[20] In a CO_2 transport simulation using GEOS-4 and the NASA finite volume data assimilation system (FVDAS) fields to drive an offline chemical transport model (CTM),

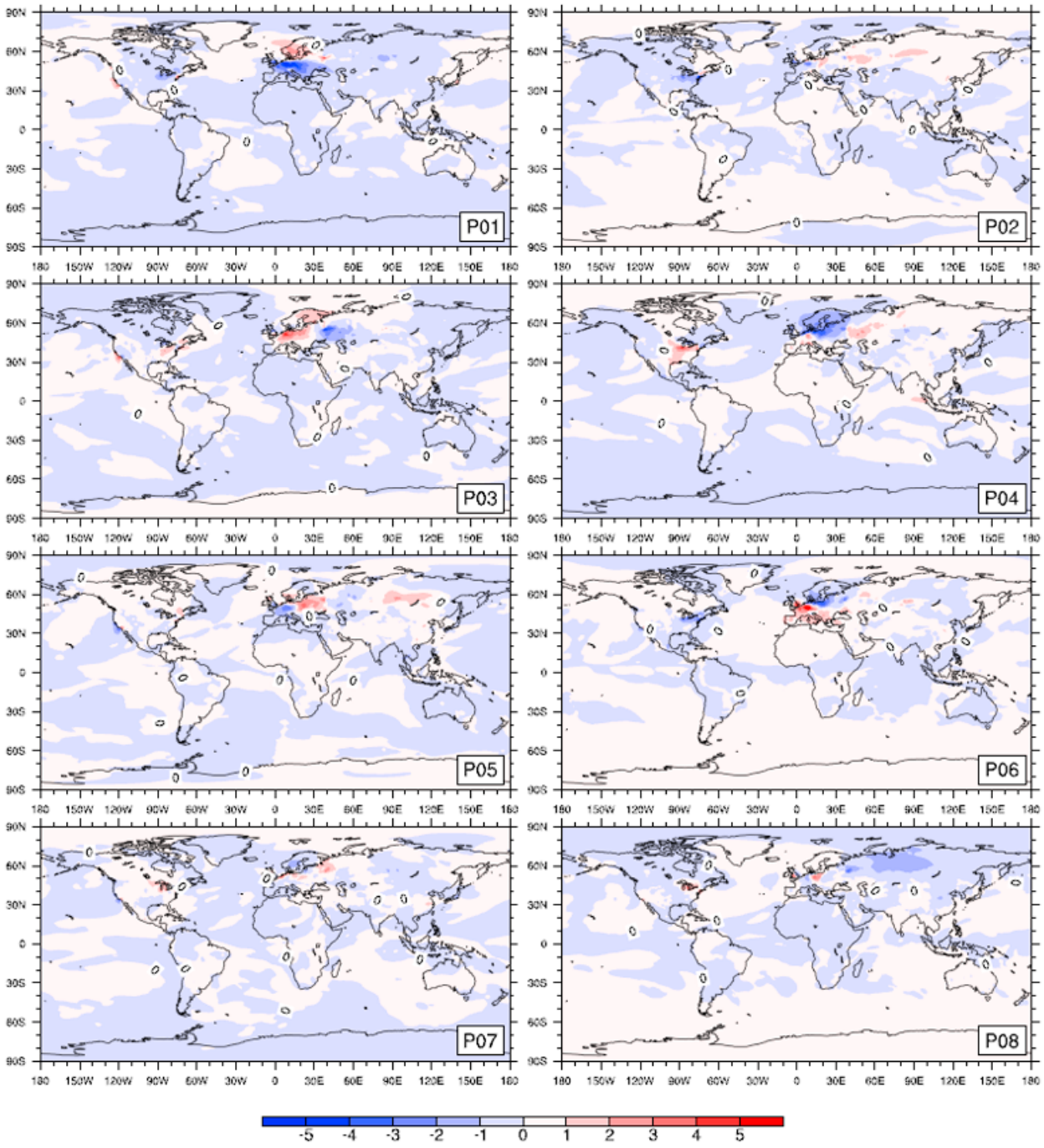

Figure 3. December, 2001, CO_2 from fossil fuel (parts per million): global values for deviations from the eight-ensemble mean. Maximum deviations occur at the dark blue and dark red locations.

Kawa et al. [2004] found that the tracer was not conserved during advection and convection. It was determined that the reason for this discrepancy was that the DAS meteorological data, in which the surface pressure tendency and mass flux convergence were not always consistent, lead to errors in the predicted surface pressure. Both a "pressure fixer" and a new convective transport module were added to the offline CTM at that time to improve results. Even for that generation of model it was recognized that there is large sensitivity to transport in certain regions, which likely affects model error covariances used in inversions and that some parts of the globe are likely to experience larger CO_2 variations, because of long-range transport, than are others. We investigate remaining effects of differing time-dependent transport patterns using free-running simulations, which have the advantage of conserving mass, as a result of differing initial conditions in GEOS-5.

[21] Figure 4 shows that Northern Hemisphere CO_2 cycles simulated by the model are generally in phase with the data provided by CarbonTracker although the amplitudes are

Table 1. Mean and Maximum Percent (Expressed as Fraction) Deviations From Ensemble Mean Values[a]

Ensemble Member	Mean Deviation Jan 2000	Max Deviation Jan 2000	Mean Deviation Dec 2001	Max Deviation Dec 2001
P01	0.0010447779	0.1987460532	−0.0024473974	0.1390163346
P02	−0.0007079733	0.1594262739	0.0010350785	0.0701868561
P03	−0.0001030051	0.1015154389	−0.0005215160	0.1248158015
P04	9.8400155e-05	0.2117673279	0.0004498687	0.1444526864
P05	−0.0003401078	0.2023678019	0.0003891951	0.1083048087
P06	−0.0011610277	0.0788179804	0.0026228091	0.2250762132
P07	0.0011200552	0.1791553609	0.0001354068	0.1088921124
P08	4.8880779e-05	0.1472506528	−0.0016634449	0.1099138499

[a]The largest (P04) and smallest (P06) maximum percent deviations (expressed as fractional amounts) from the mean for January, 2000 differ by a factor of 3. The largest maximum percent deviation for December 2001 (P02) is also 3 times the smallest (P06). Mean percent deviation from the mean for all simulations, while low and somewhat variable, persists from the first month of the run until the last, suggesting that the simulations tend not to further converge to the mean in two years' time.

underestimated by the model at both Romania and Kazakhstan, and the June 2000 minimum for the CarbonTracker data in Romania leads the simulations by one month. Model amplitudes at Park Falls, Wisconsin overestimate the CarbonTracker data especially during the latter half of 2000 and at the July–August minimum in 2001. At Mauna Loa, the models show slightly larger amplitudes but very similar phasing for 2000, and very near matches for amplitude and phase in 2001. These similarities among model runs and observations suggest that both physical parameterizations and CO_2 flux sources are administered reasonably for the Northern Hemisphere and that the differing initial conditions in meteorology in the eight ensemble runs have little effect on the realization of the CO_2 cycle at these latitudes.

[22] Results for the Southern Hemisphere in Figure 5 show marked differences in both amplitude and phasing among the models and with regard to the observational data set. In fact, the number of months difference in phase for models compared to observations differs according to latitude—the farther north in the southern hemisphere, the farther out of phase. For example, at Easter Island (coordinates: 27.15S, 109.45W), the simulations lead the observations by four months; at Cape Grim, Tasmania (40.68S, 143.68E), by three months; at Maquarie Island (54.48S, 158.97E), by one month; and at the South Pole by less than a month.

[23] To better understand the cause of the widely differing model simulations for Cape Grim, the FFT procedure performed on the total CO_2 cycle for all of the locations in the study was employed for each component of the total CO_2 concentration at Cape Grim and compared to the CarbonTracker data for the region. Figure 6 shows that biomass burning has little effect on the cycle, that the ocean cycle leads the observations by three months (as found by *Kawa et al.* [2004]), and that both the terrestrial biosphere (CASA) and the fossil fuel cycles are affected quite differently by the propagation of the differing initial meteorological conditions applied to each model ensemble member. It should be noted, however, that local discrepancies in the CASA data itself may contribute to the differences seen among the simulations for this component—a point demonstrated by *Masarie et al.* [2011] when bias was introduced into Park Falls, Wisconsin data input into a CO_2 flux simulation.

[24] The fossil fuel component of the CO_2 cycle here is the only component that is more or less in phase with the observations (especially for ensemble members P01 and P02, identical for this component and represented by the red curve), which is consistent with *Kawa et al.* [2004]. The amplitude of this signal is approximately 30% of the total CO_2 signal in the observations, consistent with *Erickson et al.* [2008] in which the National Center for Atmospheric Research (NCAR) Community Atmosphere Model, Version 4.0, was run with a monthly fossil fuel flux data set from *Andres et al.* [1996]. These findings suggest that although interhemispheric transport of CO_2 from fossil fuel from the Northern Hemisphere to the Southern Hemisphere may affect the phase of the CO_2 cycle in the Southern Hemisphere; internal model variability still obstructs the true fossil fuel CO_2 signal at specific sites in the Southern Hemisphere.

3.3. Interhemispheric Exchange Time

[25] Observations of long-lived tracers indicate that the time required for mixing tropospheric air between the Northern and Southern Hemisphere extratropics is on the order of 0.61–1.4 year [*Kawa et al.*, 2004; *Denning et al.*, 1999; *Bowman and Cohen*, 1997; *Heimann and Keeling*, 1986]. Using the adapted Bowman and Cohen equations (1) and (2) above, we obtain the values shown in Table 2 for the lowest atmospheric layer concentrations of CO_2 for each of the eight simulations from 2000 to 2001 and for each of the four different sources of CO_2. Remaining mindful that this box model calculation accounts only for Northern Hemisphere sources, we note the following interhemispheric transport values obtained. For Total CO_2 (CO2TOT), transport time ranges from 0.93 yr. to 1.06 yr, a value slightly less than that of *Heimann and Keeling* [1986], but in keeping with *Denning et al.* [1999]. The CO_2 from fossil fuel burning (CO2FF) transport time range is 0.442 yr. to 0.456 yr.—significantly less than values seen for total CO_2 in this or in any other model. Terrestrial Biosphere CO_2 (CASA) transport time shows the widest range from −9.26 yr. to 1.43 yrs. (The two negative source values here are due to the fact that CASA is artificially balanced annually to be close to zero, and thus gives source values slightly above or slightly below zero). Four of the terrestrial biosphere simulations (P03, P04, P05, and P07), however, show transport time between 0.01 yr. and 0.1 yr. (approximately 3–37 days). Ocean CO_2 (CO2OCN) values represent Northern Hemisphere sinks and resulting removal of CO_2 from the Southern Hemisphere with "transport" time of 1.5 yr. Differences in transport times among the various constituent source/sinks of total

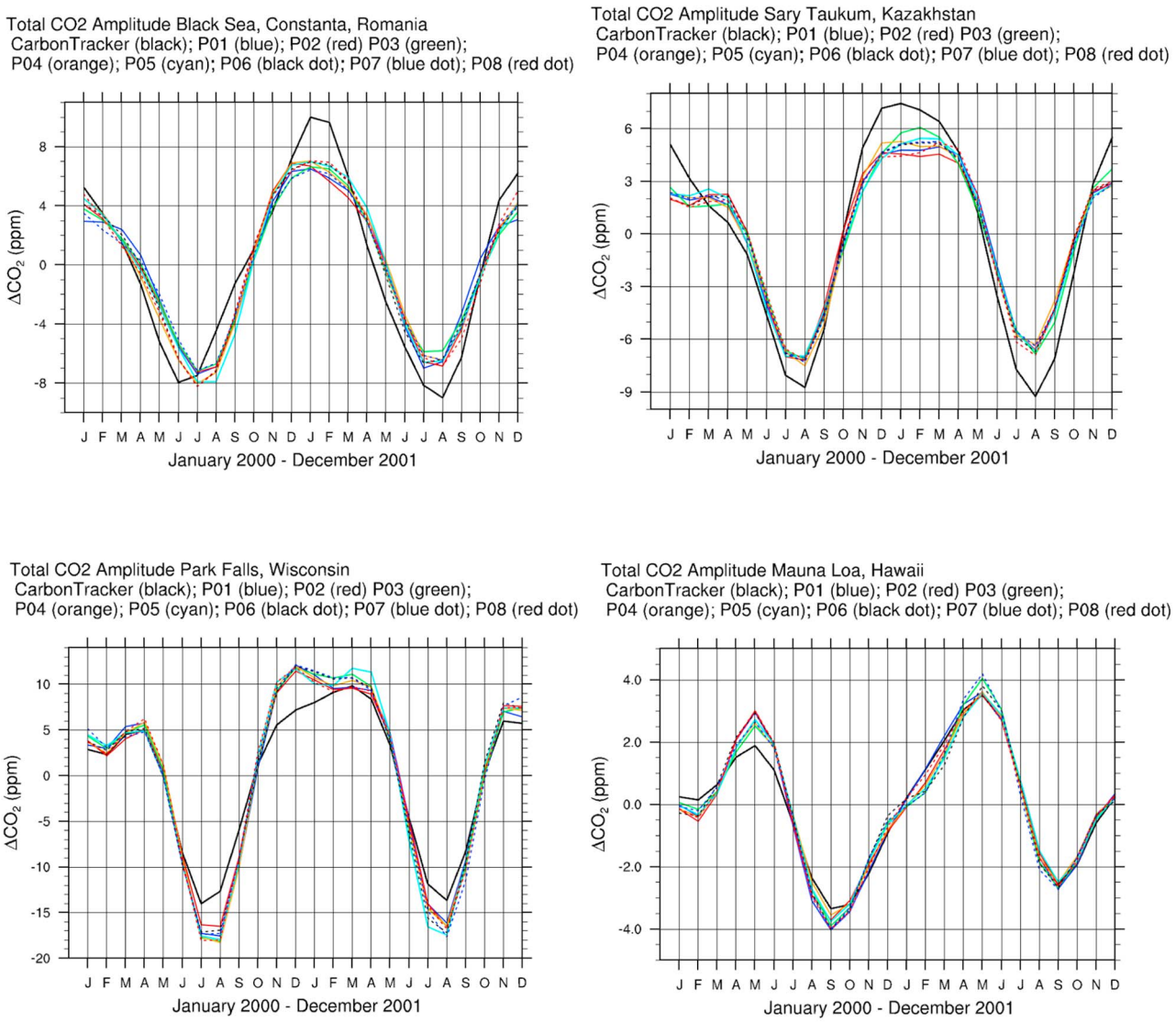

Figure 4. Northern Hemisphere total CO_2 (composite of sources from ocean, terrestrial biosphere, fossil fuel emissions and biomass burning) seasonal amplitude 2000–2001, CarbonTracker versus GEOS-5 ensemble (note different ranges for different y-axes). Northern Hemisphere CO_2 cycles simulated by the model are generally in phase with the CarbonTracker data although the amplitudes are underestimated by the model at both Romania (44.17°N, 26.68°E) and Kazakhstan (44.45°N, 75.57°E), and the June 2000 minimum for observations in Romania leads the model simulations by one month. Model amplitudes at Park Falls, Wisconsin (45.95°N, 90.27°W) overestimate observations especially during the latter half of 2000 and at the July–August minimum in 2001. At Mauna Loa (19.53°N, 155.58°W), the model simulations show slightly larger amplitudes but very similar phasing for 2000, and very near matches for amplitude and phase in 2001.

CO_2 may be due to their proximal distribution about the equator.

3.3.1. Vertical Transport

[26] *Denning et al.* [1998], found that differences in vertical structure among general circulation models dominate the differences in true interhemispheric exchange. To investigate differences in vertical structures developed from initial conditions that may be responsible for similar transport discrepancies within the GEOS-5 model, we examine transport time at the 500 mb level. Table 3 shows the outcome of these calculations. The results show a wider range of values at this level than at the surface level, suggesting large discrepancies in the vertical mixing in each of the simulations. In this case, Total CO_2 (500TOT), transport time ranges from 0.83 yr. to 0.95 yr. For CO_2 from fossil fuel burning (500FF), the transport time range is about twice as long at the 500 mb level than it is at the surface: 0.83 yr to 1.09 yr and represents a 31% increase from the smallest to the largest value as compared to only a 3% increase from smallest to largest surface values. Terrestrial Biosphere CO_2 (CASA) transport time again shows the widest range at this level from 0.167 yr to 1.58 yr (rejecting the 11 yr. outlier). The range of ocean CO_2 (CO2OCN) values range from 0.446 yrs to 1.03 yrs.

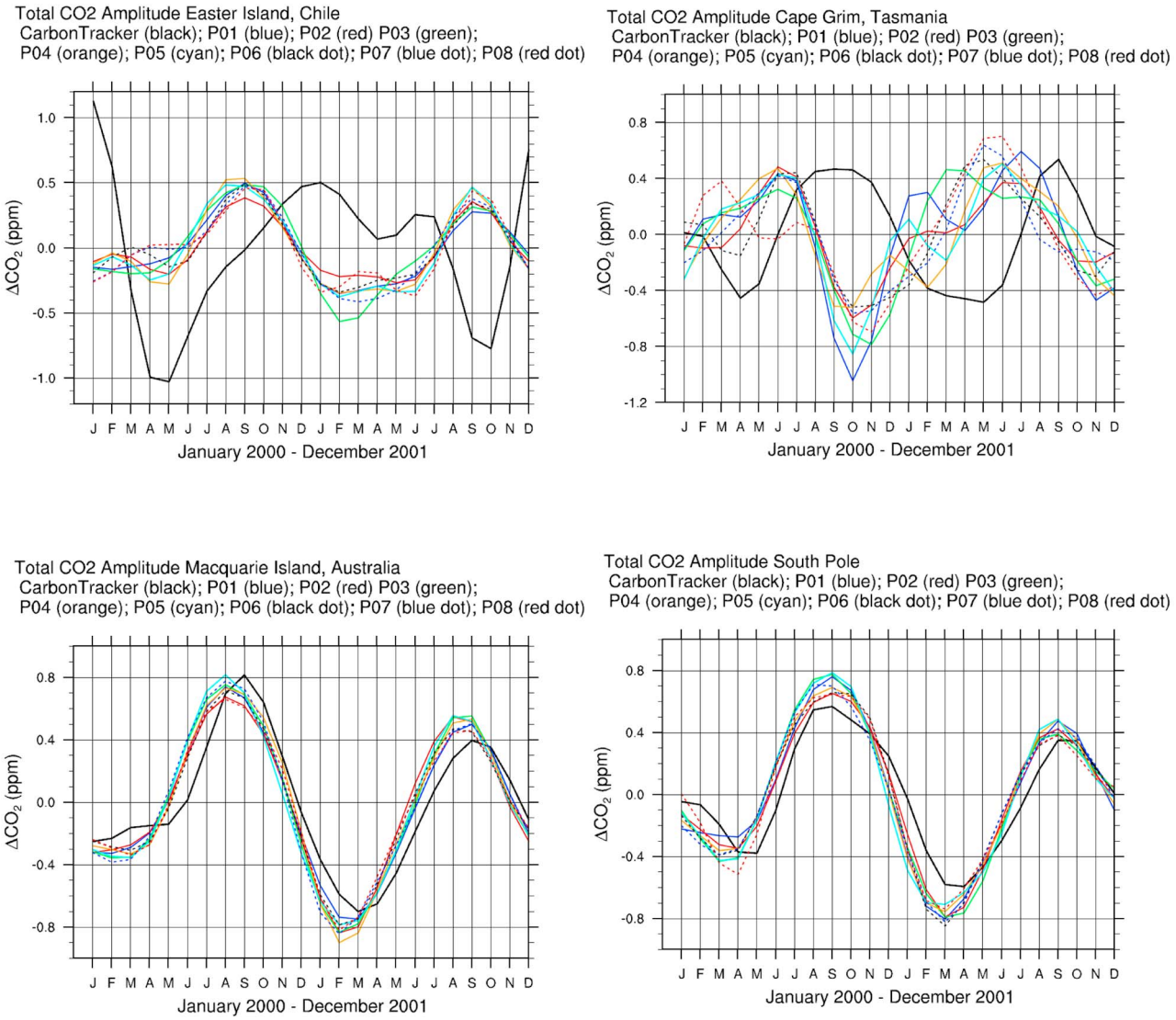

Figure 5. Southern Hemisphere total CO_2 seasonal amplitude 2000–2001 Observations versus GEOS-5 ensemble. CO_2 cycle results for the Southern Hemisphere show marked differences in both amplitude and phasing among the models and with regard to the CarbonTracker data sets. At Easter Island (27.15°S, 109.45°W) the simulations lead the observations by four months; at Cape Grim, Tasmania (40.68°S, 143.68°E), by three months; at Maquarie Island (54.48°S, 158.97°E), by one month; and at the South Pole (89.98°S, 24.8°W) by less than a month.

[27] In the TRANSCOM studies conducted by *Law et al.* [1996], results from twelve atmospheric transport models were collected and analyzed for differences in representation of CO_2 transport. Within this study, an assessment of the large discrepancy in interhemispheric concentration differences between the model that produced the largest difference and the one that produced the smallest revealed that there were differences in the models' subgrid scale vertical transport mechanisms, and were the result of the different parameterizations used and the different numerical diffusion properties of the advection schemes in the two models. In the study it was noted that one of the models investigated appeared to have weak vertical mixing throughout the troposphere while another had weak mixing out of its surface layer. In both models, this resulted in higher surface concentrations. While the range of transport times found in the different simulations of the single GEOS-5 model is not quite as large a range as that of the *Law et al.* [1996] multiple model comparison, it suggests that surface mixing strength over the time span of a model run may vary for sensitive regions in the model. Additionally, the observation that the transport times for each component of the CO_2 signal range from 0.01 yr to 1.58 yr indicates that while the various components undergo essentially the same mixing processes, there are differences in the resulting spatial structure of the CO_2 tracer that are being driven by mixing processes (i.e., timing and strengths of fronts and planetary waves). To gain insight into the effect of transport processes on atmospheric flow from the Northern Hemisphere to the Southern Hemisphere, a 3D time-varying flow analysis was performed using a method of integration-based flow analysis.

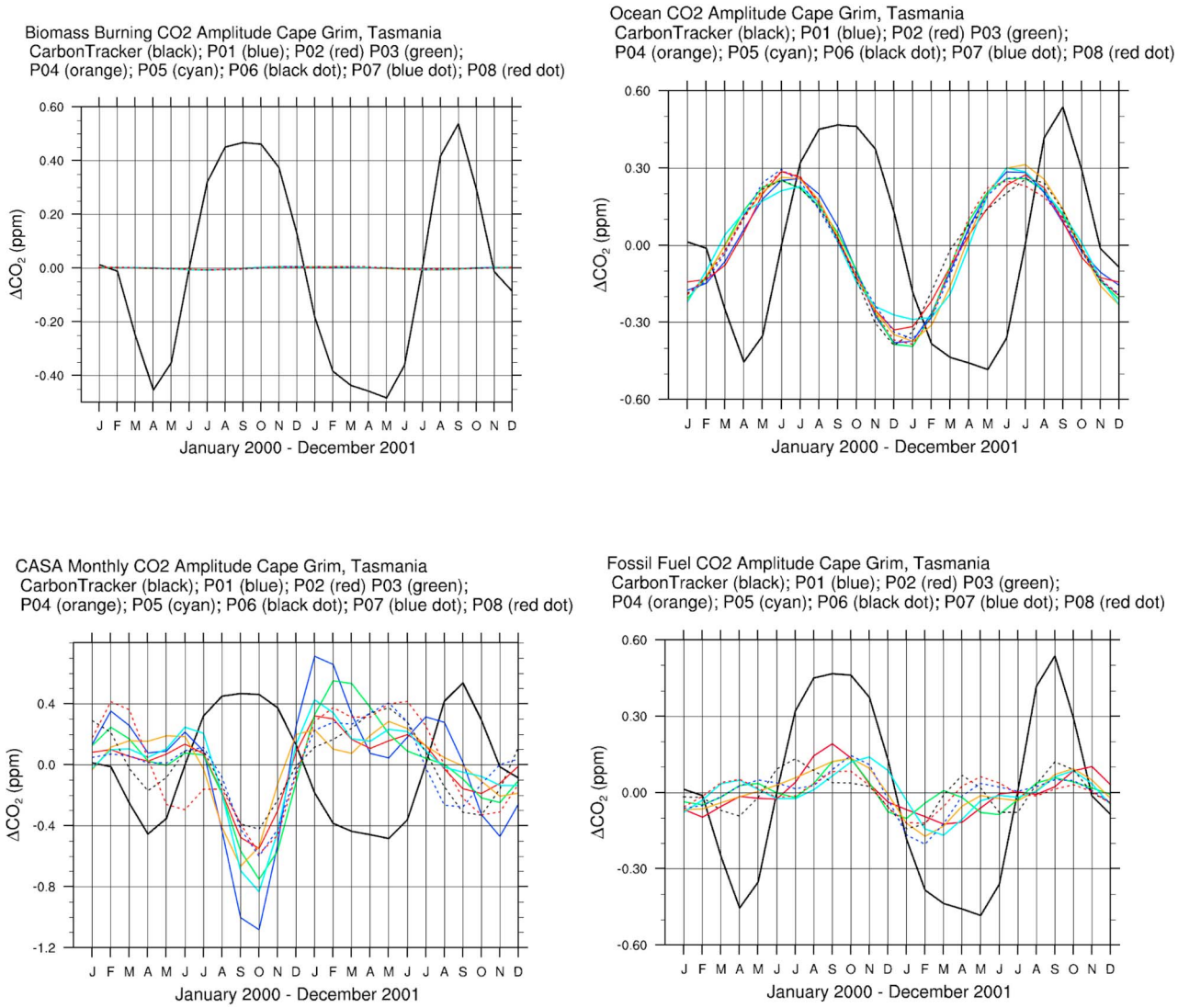

Figure 6. Cape Grim (40.68°S, 143.68°E) components of the CO_2 cycle. Biomass burning has little effect on the cycle, the ocean leads the observations by three months (as in *Kawa et al.* [2004]), and both the terrestrial biosphere (CASA) and the fossil fuel cycles are affected quite differently by the internal model variability with regard to the development of the differing initial meteorological conditions applied to each ensemble member.

3.4. Flow Into Mauna Loa

[28] In their twelve-model inter-comparison project, *Law et al.* [1996] determined that large-scale winds account for about half the difference between model results, and that additional attribution must lay in differences in the subgrid scale vertical transport parameterization and diffusion

Table 2. Northern Source (S_N in mol/mol) and Interhemispheric Transport Time (yrs), Surface[a]

S_N CO2TOT	Tau CO2TOT	S_N CO2FF	Tau CO2FF	S_N CO2CASA	Tau CO2CASA	S_N CO2OCN	Tau CO2OCN	Ensemble Member
4.86E-06	0.951	8.76E-06	0.445	1.12E-07	1.43	−1.26E-06	1.32	P01
4.61E-06	1.06	8.58E-06	0.456	−7.00E-09	−9.26	−1.21E-06	1.39	P02
4.95E-06	0.939	8.80E-06	0.444	3.26E-07	0.0601	−1.24E-06	1.32	P03
4.89E-06	0.965	8.74E-06	0.449	1.71E-07	0.105	−1.02E-06	1.58	P04
5.10E-06	0.926	8.89E-06	0.441	2.69E-07	0.0156	−1.22E-06	1.38	P05
4.75E-06	1.01	8.81E-06	0.444	−9.40E-09	−2.77	−1.16E-06	1.43	P06
4.78E-06	0.970	8.83E-06	0.437	1.47E-07	0.0545	−1.20E-06	1.26	P07
4.95E-06	0.952	8.83E-06	0.442	1.06E-07	0.313	−1.11E-06	1.54	P08

[a]Total CO_2, CO_2 from fossil fuel, terrestrial biosphere CO_2, and ocean CO_2 for all eight simulations are shown for the lowest atmospheric layer in the model. Northern Hemisphere source CO_2 (S_N) is given in mol/mol values. Interhemispheric transport time Tau is given in year fraction.

Table 3. Northern Source (S_N in mol/mol) and Interhemispheric Transport Time (yrs), 500 mb[a]

Sn 500TOT	Tau 500TOT	Sn 500FF	Tau 500FF	Sn 500CASA	Tau 500CASA	Sn 500OCN	Tau 500OCN	Ensemble Member
3.90E-06	0.894	8.43E-06	0.831	−2.66E-08	0.519	−2.18E-06	0.482	P01
3.79E-06	0.952	7.40E-06	0.887	−1.28E-08	−0.188	−2.10E-06	0.446	P02
4.08E-06	0.902	8.51E-06	0.821	−3.72E-08	0.167	−2.32E-06	0.469	P03
3.75E-06	0.954	6.50E-06	1.07	−6.20E-09	−0.581	−1.05E-06	1.03	P04
3.77E-06	0.946	6.39E-06	1.09	−4.60E-09	−2.30E-14	−1.11E-06	0.995	P05
3.65E-06	0.929	6.44E-06	1.06	2.00E-10	11.0	−1.03E-06	1.02	P06
4.08E-06	0.833	7.30E-06	0.936	−5.08E-08	0.402	6.98E-01	−1.47E-06	P07
3.91E-06	0.881	6.76E-06	1.02	−5.60E-09	−0.0714	−1.62E-06	0.691	P08

[a]Total CO_2, CO_2 from fossil fuel, terrestrial biosphere CO_2 and ocean CO_2 for all eight simulations are shown for the 500 mb atmospheric layer in the model. Units are as in Table 2.

properties of their advection schemes. Since the Mauna Loa observatory, at its remote location, has traditionally provided a reliable account of the background state of atmospheric CO_2, we begin by examining large-scale wind flow paths here using an integration-based flow analysis.

[29] To determine the historical path of a given particle arriving at Mauna Loa, equation (3) in section 2.3 is solved using a negative time step (=14,400 s, i.e., 4 hours), and the integration progresses backward through space and time. In these analyses the lower 13 pressure layers (approximately 1013 hPa to 820 hPa if the lowest layer is at sea level) were queried for, and particle tracers initialized from each of those queried points. This vertical limit was selected such that some vertical transport is shown along with the horizontal, but not so much as to make the plot so dense as to be incomprehensible. The destination location was set to the lower 13 pressure layers of Mauna Loa.

[30] Observations from CarbonTracker (Figure 4) showed that maximum CO_2 mixing ratios occur in May of 2000 and May of 2001 and that minimum values occur in September 2000 and 2001. Aside from an increase in the amplitude of CO_2 at Mauna Loa from 2000 to 2001, no remarkable differences in transport are seen from one year to the next at this location. We present examples of particle flow with three-month lead time into Mauna Loa for the year 2001 for these months. All simulations at this location estimate well both amplitude and phasing of the CO_2 cycle for the period. For the remainder of the figures in this paper, each color represents the trajectory computed by each model simulation. Opacity corresponds to time elapsed—the more transparent, the longer temporal displacement.

[31] As can be seen in Figures 7 and 8 (May and September, 2001 particle flow with three-months' lead time into Mauna Loa, respectively), the Hadley circulation contributes to the interhemispheric transport through its seasonal oscillation [*Bowman and Cohen*, 1997]. In response to seasonal solar heating, the Intertropical Convergence Zone (ITCZ) moves northward and southward (toward the warmer hemisphere), allowing air that was previously in one Hadley cell to be carried upward and poleward in the other Hadley cell. Additionally, transport within convective cells (such as those characteristic of tropical cyclones) increases the rate at which tracers are transported between adjacent convective rolls [*Young et al.*, 1989]. Therefore, it might be assumed that the CO_2 cycle at locations receiving Hadley cell air should be affected by surface sources in the other hemisphere. Mauna Loa is one such location.

[32] At three months in advance of May 2001 arrival, Figure 7 shows that sources of air entering Mauna Loa include air from vortices located at 30°S. These sources are swept into the equatorial current and then drawn into the Pacific vortex before entering Mauna Loa. Air particles that begin in the Southern Hemisphere follow a vertical pathway into the Northern Hemisphere. At one month lead time, particles are generally near the northeastern U.S. coastline. From there, they either follow the jet stream to the Atlantic and over Eurasia, to enter from the Pacific, or they travel southward over the Atlantic, as in P03-P08, to be drawn into Mauna Loa across North America.

[33] In Figure 8, arrival at Mauna Loa in September, 2001 with three month lead time is shown. As the ITCZ and the jet stream move south, the jet stream plays less a role in an airstream's travel into Mauna Loa than it does in May. At three months in advance of arrival, southern sources of air also undergo less activity in September than they do in May. Interhemispheric exchange occurs mainly in the region between eastern Africa and Indonesia. Northern paths originate in North America and the Atlantic Ocean. No Southern Hemisphere sources appear in P07. Few are included in P01. Again, the interhemispheric transport is seen to be accomplished mainly by travel in the upper atmospheric layers.

[34] In the case of the CO_2 cycle at Mauna Loa, all eight simulations are in phase with observations and within a few ppm of the amplitude. In both May and September, all simulations follow similar one-month lead time paths to Mauna Loa. Northern Hemisphere sources (eastern Canada and the Atlantic Ocean) three months before arrival are similar for all models while Southern Hemisphere sources either vary or are not present. This suggests that Northern Hemisphere sources of air (and consequently, CO_2) have a larger effect on the amplitude and the phasing of the carbon cycle at Mauna Loa than Southern Hemisphere sources do. Thus, varying initial meteorological conditions in GEOS-5 does not produce a large effect on CO_2 concentrations at Mauna Loa. Northern Hemisphere sources, which are far distant from Mauna Loa, are well-mixed by the time they reach Mauna Loa, so they affect concentration there similarly in all simulations. Southern Hemisphere sources are few, so variations in transport times for particles from these locations have little effect on CO_2 concentrations at Mauna Loa.

3.5. Flow Into Cape Grim

[35] At Cape Grim, Tasmania, observations showed that minimum CO_2 mixing ratios occur in April of 2000 and May

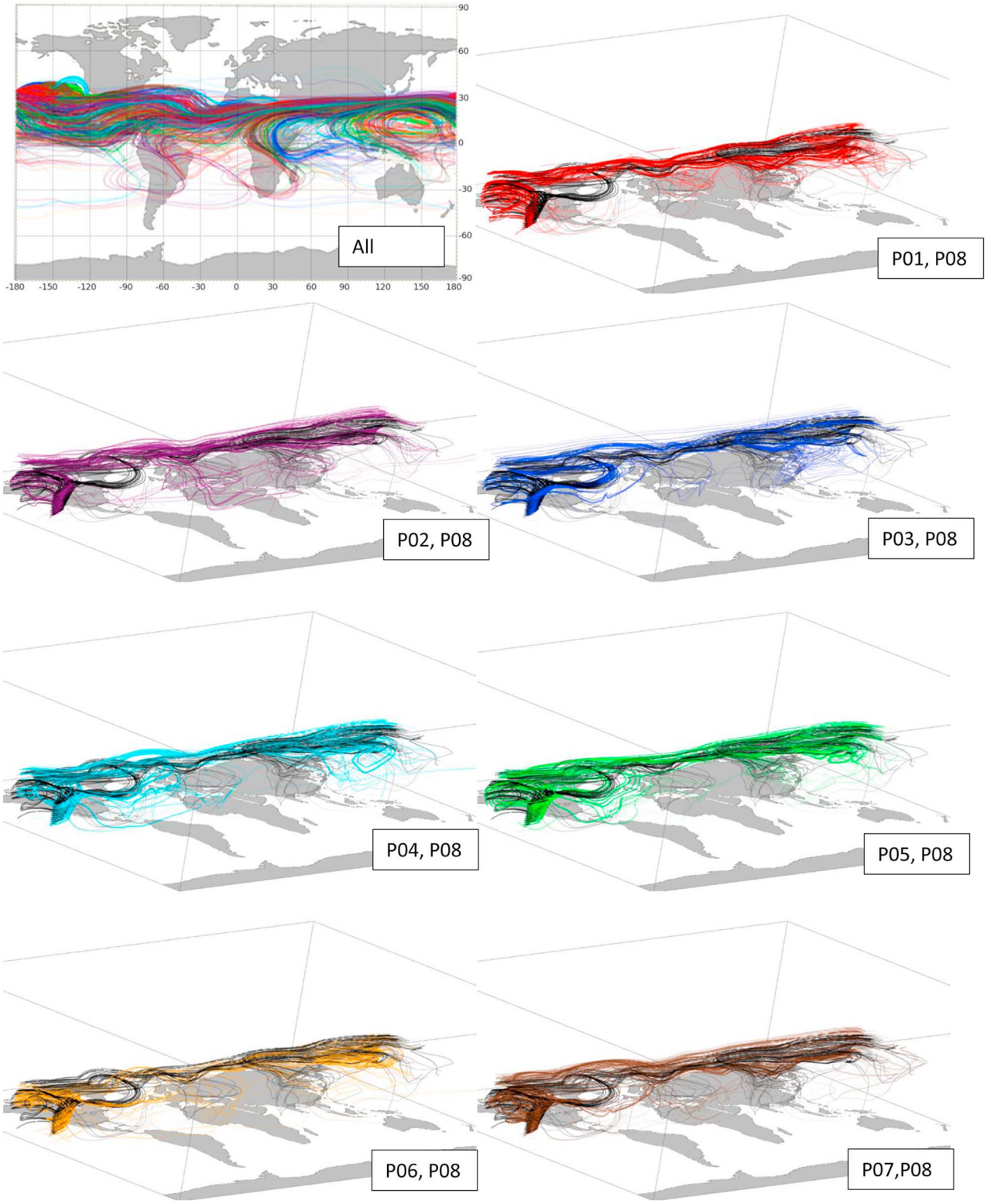

Figure 7. May 2001 arrivals into Mauna Loa (19.53°N, 155.58°W) with three month lead times. Opacity corresponds to time elapsed—the more transparent, the longer temporal displacement. At three months before arrival, sources of air entering Mauna Loa include air from vortices located at 30°S. These sources are swept into the equatorial current and then drawn into the Pacific vortex before entering Mauna Loa. Air particles that begin in the Southern Hemisphere follow a vertical pathway into the Northern Hemisphere.

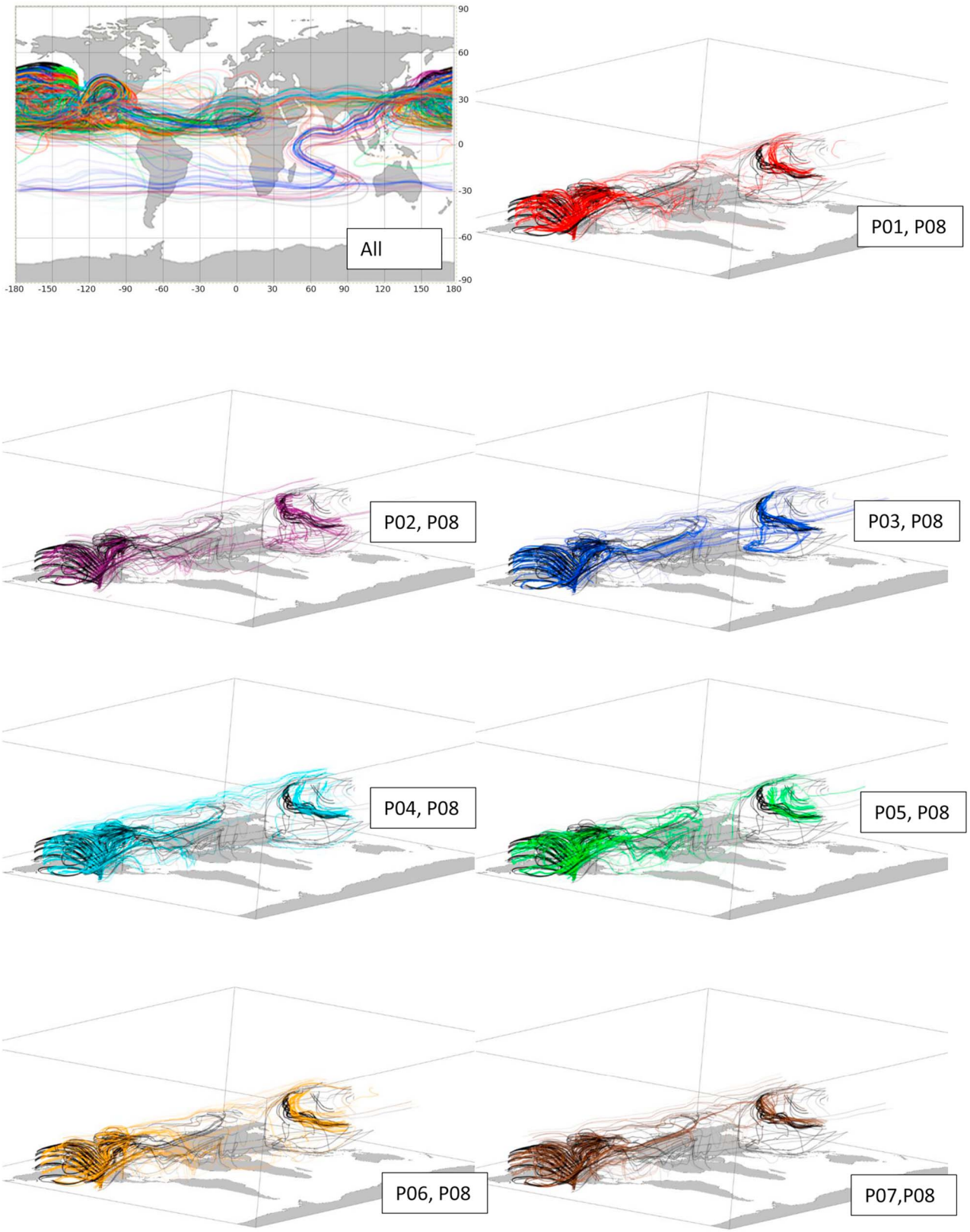

Figure 8. September 2001 arrivals into Mauna Loa (19.53°N, 155.58°W) with three month lead times. As the ITCZ and the jet stream move south, the jet stream plays less a role in an airstream's travel into Mauna Loa than it does in May. Interhemispheric exchange occurs mainly in the region between eastern Africa and Indonesia. Northern paths originate in North America and the Atlantic Ocean. No Southern Hemisphere sources appear in P07. Few are included in P01.

of 2001 and that maximum values occur in September 2000 and 2001. This cycle is the reverse of that of Mauna Loa.

[36] Since this is where the largest discrepancies in the CO_2 cycle were found among the GEOS-5 simulations, we investigate the large-scale processes in this region in comparison with those at the more stable Mauna Loa site using flow analysis into this region in May and September. It should be noted that our results are not the first to show prominent differences between observations and model output for tracer concentrations in the Australian region. Several studies have shown southern midlatitude tracer concentration aberrations in their findings. A few are described in the following section.

3.6. Known Australian Regional Aberrations

[37] The *Conway et al.* [1994] study evaluating CO_2 flask data noted that in the Southern Hemisphere, Cape Grim, Tasmania concentrations of CO_2 always fell below that which was calculated using the cubic polynomial fit curve which approximated well the northern to southern hemisphere CO_2 gradient. This location consistently showed the lowest annual mean in the observational network with values slightly lower even than those at the South Pole.

[38] In the *Law et al.* [2003] TRANSCOM 3 CO_2 inversion comparison, data network tests performed showed that only the Australian region source estimates varied over a much larger range than that given by the established control case uncertainty estimate. By their estimation, the data suggested that the assumed spatial pattern of sources in Australia in the 16 models compared was incorrect—that larger sources were required in the northern part of the continent relative to the south. An alternative explanation, that there could be an error in transport, was deemed less likely since all transport models behaved in the same way. We propose that this region may indeed pose a transport challenge for many models based on internal model variability.

[39] A look at the flow patterns of individual ensemble member simulations for May and September, 2001, at three month lead time reveals significant differences in particle pathways into Cape Grim. In Figure 9, May 2001 arrivals into Cape Grim with three month lead time, simulations show streamlines coming primarily from the Atlantic, Africa and southern Asia. P01, P02, P04 and P07 include paths taken through North America. Simulations P05-P08 include an Atlantic vortex into which Northern Hemisphere air is drawn to be delivered to the Southern Hemisphere. Long-range particles are carried primarily in the uppermost vertical layer (~820 hPa). Figure 10 shows September 2001 arrivals into Cape Grim with three month lead time. Peak CO_2 values for the observation data occur during this month, while all of the GEOS-5 model simulations are in the middle of CO_2 decline here. Lowest CO_2 fossil fuel values occur in September 2001 for P08. This is also the only simulation for which the Southern Ocean air current is the only source of airstreams. Highest GEOS-5 model values during this month obtain for P01, P04, P05. The most varied paths to Cape Grim are taken by simulations P02, P03, P06 and P07. Interhemispheric transport paths are seen mainly in the upper atmospheric layers. We recall that the model simulations whose fossil fuel emission component most closely matched the phasing of the Cape Grim CO_2 cycle were P01 and P02 and that these were the only two to show residence in southeast Asia, a known major emitter of fossil fuel CO_2.

3.7. Interannual Variability

[40] In addition to the variability among the GEOS-5 model simulations for Cape Grim for each of the two years simulated, a notable amount of interannual variability was present. This result is consistent with the findings of *Conway et al.* [1994] who report significant interannual variations in the interhemispheric gradient of atmospheric CO_2 in the observation network. Figure 11 depicts May 2000 (top) and 2001 (bottom) arrivals into Cape Grim with one month lead time. Streams from blue (P03), purple (P02), red (P01) and cyan (P04) arrive latest, since these come from the largest distances away. In the 2000 simulation, black (P08) is in the African cape one month before arrival, it then travels around a South Pacific vortex before entering Cape Grim. In the 2001 simulation, black (P08) spins in a tight vortex around Tasmania while the other simulations rotate nearer the southern Australian coast. These interannual variations may be due to seasonal cyclonic activity in the Indian Ocean [*Bowman and Cohen*, 1997] or to climatic oscillations such as the El Niño/La Niña cycle. In either case, this variability is seen in only some of the simulations suggesting that meteorological differences from year to year represent only part of the variability in the simulations.

[41] September 2000, 2001 arrivals into Cape Grim with one month lead time are shown in Figure 12. Here we see more interannual variability in more of the simulations. In 2000, black (P08) and yellow (P06) curl around the African cape one month before arrival, while in 2001, red (P01) and blue (P03) show this pattern. Blue (P03), cyan (P04) and green (P05) spin near the southern Australian coast in 2000, but only green (P05) does this in 2001.

3.8. El Niño/La Niña

[42] Much interannual variability is related to natural climate fluctuations. For instance, the effect of El Niño/La Niña, can be large compared to the effect of changes in annual fossil fuel emissions [*Conway et al.*, 1994]. In fact, the terrestrial biosphere releases more CO_2 to the atmosphere during El Niño events, which results in increased CO_2 growth rates during these events [*Keeling et al.*, 1989] and La Niña events can have a slightly less and opposite effect. Results from *Heimann and Reichstein* [2008] show that the El Niño Southern Oscillation (ENSO) is in a negative phase (La Niña) in the years 2000–2001 and that during this time, the phase is becoming slightly less negative. Global background atmospheric CO_2 concentration rises only slightly (approximately 0.05 ppm) over this period.

4. Conclusions

[43] In regions of high CO_2 emissions due to fossil fuel burning, large differences among the simulations appear for both the first month and the last month of the ensemble simulation. Thus, individual simulations of an eight-member ensemble do not stabilize within a period of two years.

[44] The phasing of the CO_2 cycle at Northern Hemisphere locations in all of the ensemble members is similar to that of the CarbonTracker collection of observations, but in the southern hemisphere, GEOS-5 model cycles are out of

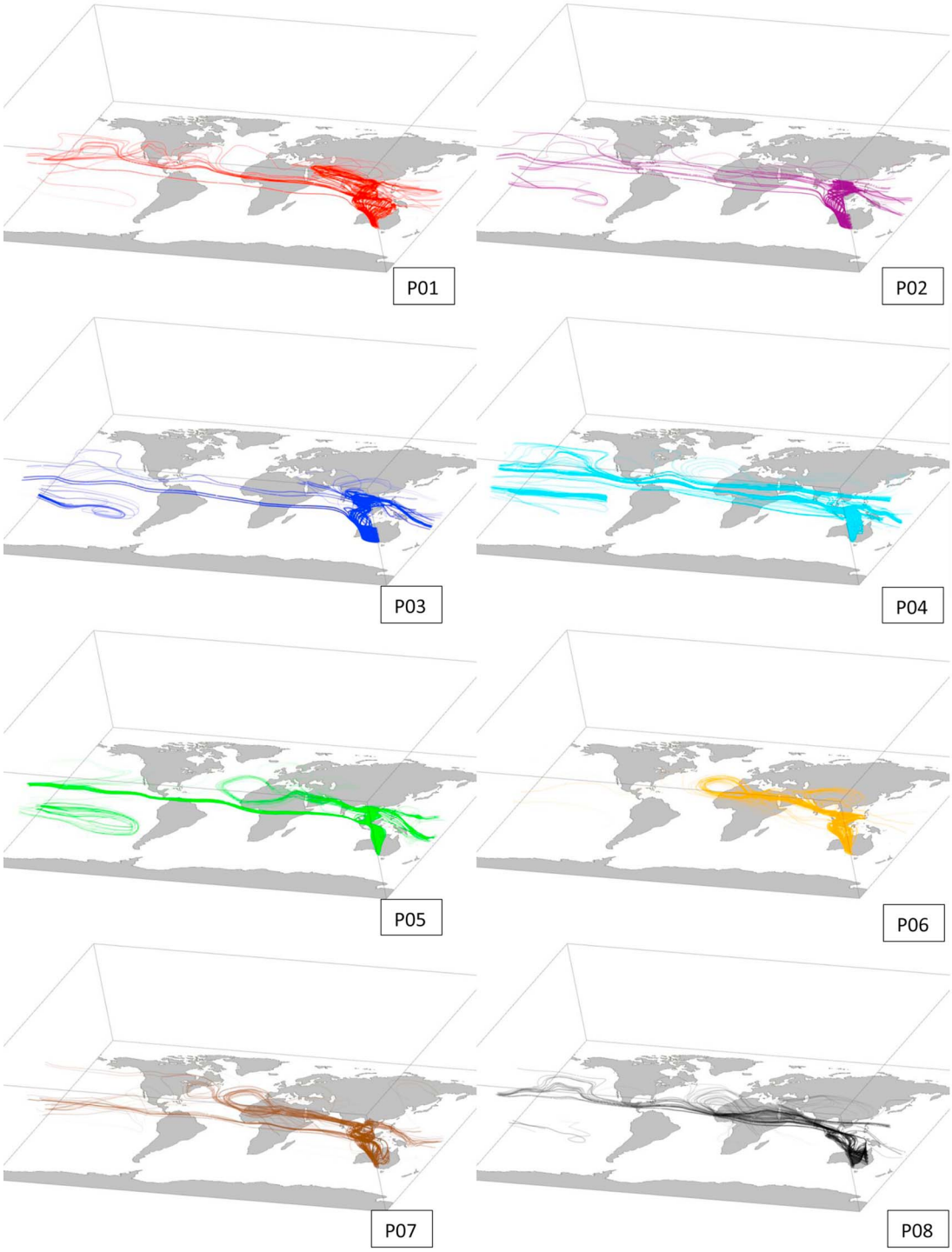

Figure 9. May 2001 arrivals into Cape Grim (40.68°S, 143.68°E) with three month lead time. Simulations show streamlines coming primarily from the Atlantic, Africa and southern Asia. P01, P02, P04 and P07 include paths taken through North America. Simulations P05-P08 include an Atlantic vortex into which Northern Hemisphere air is drawn to be delivered to the Southern Hemisphere. Long-range particles are carried primarily in the uppermost vertical layer.

phase by as much as four months, and large variations occur between the ensemble members. The most extreme differences occur among the ensemble and observational data in the Cape Grim region with regard to CO_2 uptake and respiration of the terrestrial biosphere and CO_2 emissions due to fossil fuel burning. While the amplitude of the cycle of the ocean and the terrestrial biosphere represent the largest percentages of the total CO_2 cycle at Cape Grim, the phasing of fossil fuel CO_2 at 30–40% of the amplitude most closely follows the phase of the CO_2 total at this location.

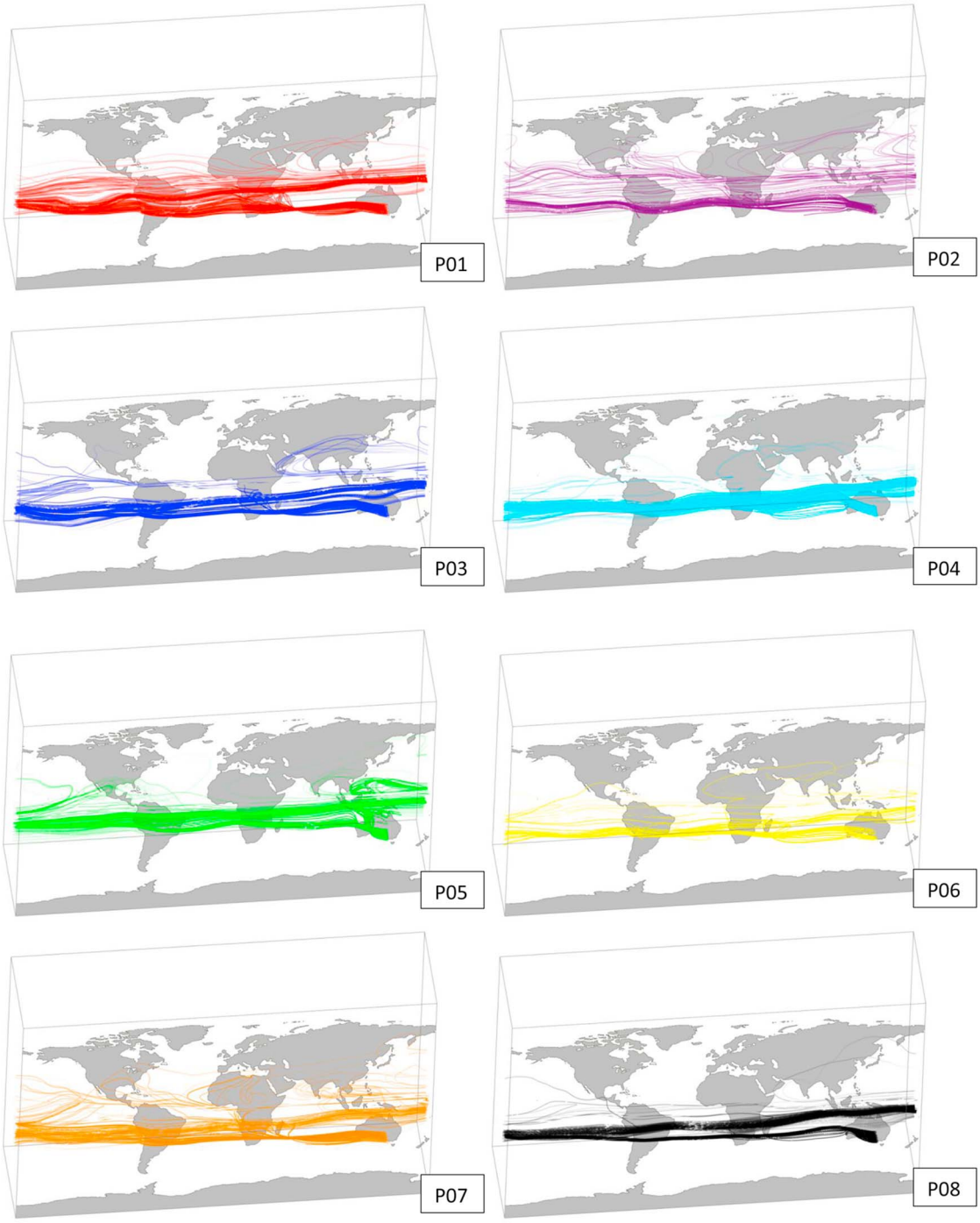

Figure 10. September 2001 arrivals into Cape Grim (40.68°S, 143.68°E) with three month lead time. Peak CO_2 values for the CarbonTracker data occur during this month, while all of the GEOS-5 model simulations are in the middle of CO_2 decline here. Lowest CO_2 fossil fuel values occur in September 2001 for P08. This is also the only model for which the Southern Ocean air current is the only source of airstreams. Highest GEOS-5 model values during this month obtain for P01, P04, P05. The most varied paths to Cape Grim are taken by simulations P02, P03, P06 and P07.

[45] These findings suggest that although interhemispheric transport of CO_2 from fossil fuel produced in the Northern Hemisphere to the Southern Hemisphere may affect the phase of the CO_2 cycle in the Southern Hemisphere, internal model variability still obstructs the true CO_2 signal at specific sites in the Southern Hemisphere. Potential explanations for these discrepancies may lie in the robustness of the terrestrial biosphere or ocean flux data, model tuning or parameterization for the Southern Hemisphere; or in that higher concentrations of CO_2 in the Northern Hemisphere

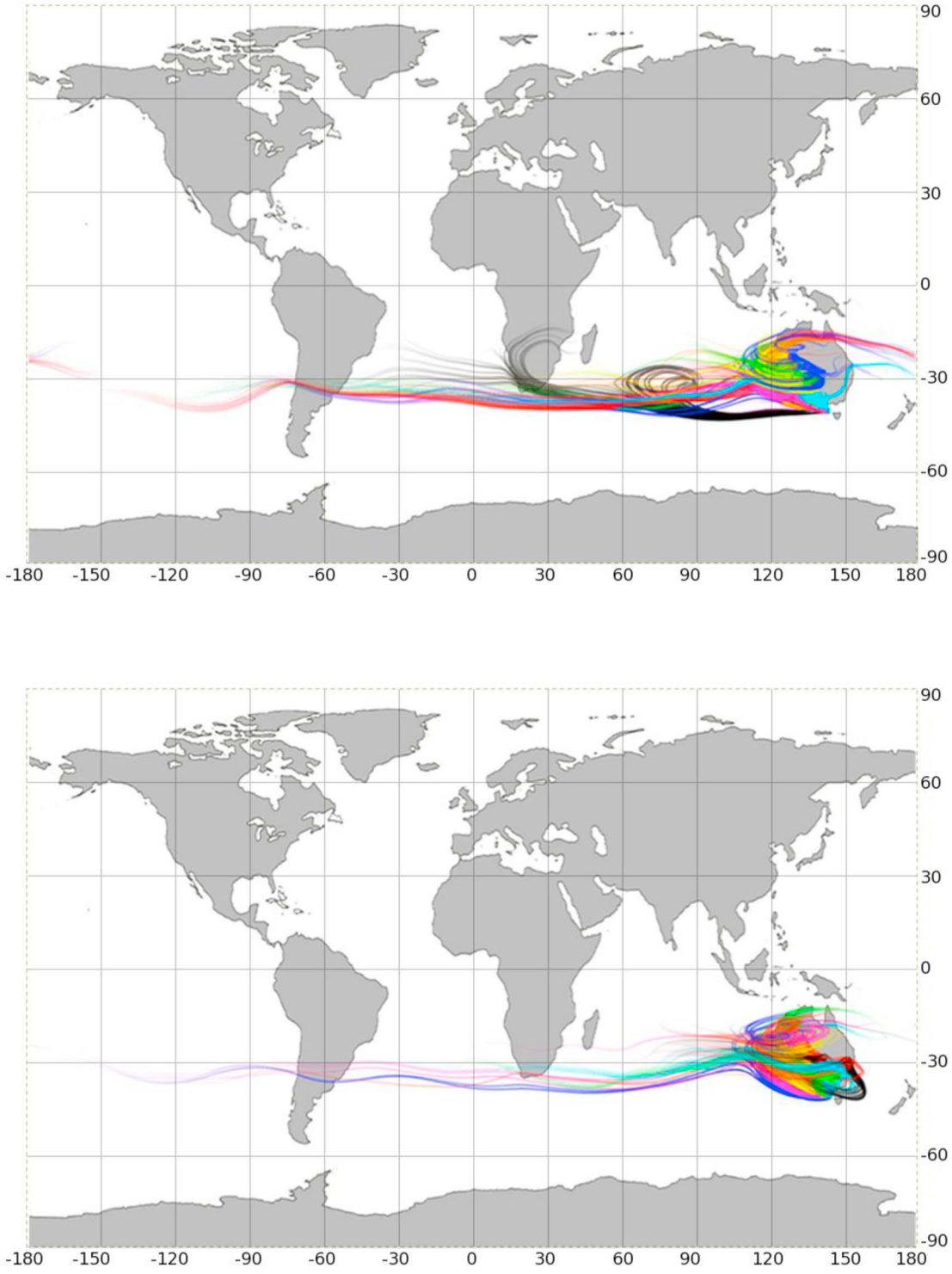

Figure 11. May (top) 2000 and (bottom) 2001 arrivals into Cape Grim (40.68°S, 143.68°E) with one month lead time. Streams from blue (P03), purple (P02), red (P01) and cyan (P04) arrive latest, since these come from the largest distances away. In the 2000 simulation, black (P08) is in the African cape one month before arrival, then travels around a South Pacific vortex before entering Cape Grim. In the 2001 simulation, black (P08) spins in a tight vortex around Tasmania while the other simulations rotate nearer the southern Australian coast. (Additional simulations: P05, green; P06, yellow; and P07, ochre).

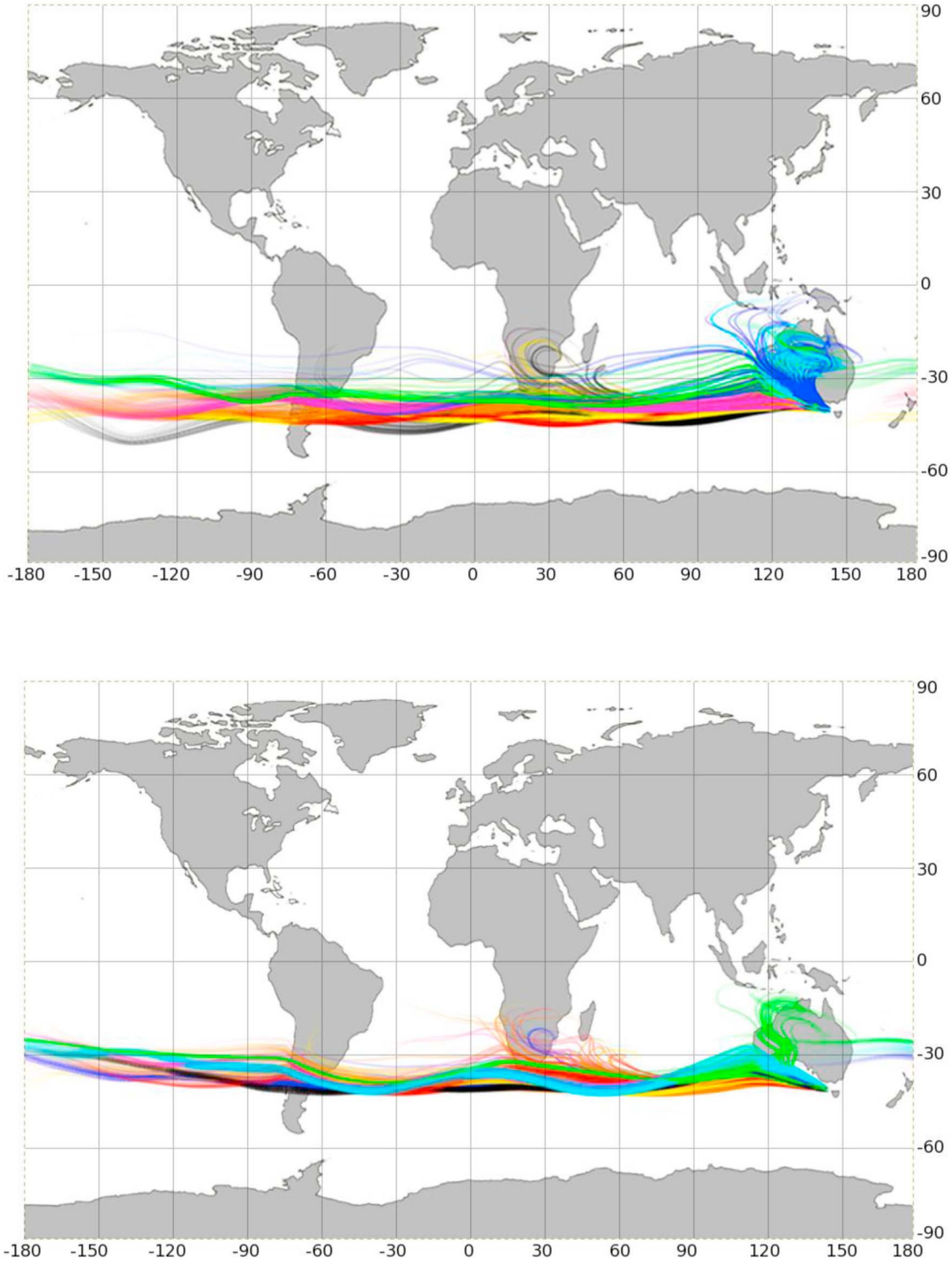

Figure 12. September (top) 2000 and (bottom) 2001 arrivals into Cape Grim (40.68°S, 143.68°E) with one month lead time. Here we see more interannual variability in more of the simulations. In 2000, black (P08) and yellow (P06) curl around the African cape one month before arrival, while in 2001, red (P01) and blue (P03) show this pattern. Blue (P03), cyan (P04) and green (P05) spin near the southern Australian coast in 2000, but only green (P05) does this in 2001. (Additional simulations: P02, purple; P07, ochre).

affect amplitude and phasing in the Southern Hemisphere more than circulation affects it in any location.

[46] It is clear that some parts of the globe experience larger CO_2 variations, due to long-range transport, than do others. Measurements in those regions might be more appropriate for monitoring CO_2 emissions than the measurements in the more stable regions, which are most efficient at monitoring the background state or trend. Furthermore, surface mixing strength over the time span of a model run may vary for sensitive regions in the model, and the large differences in the transport times for each component of the CO_2 may indicate that there are structural differences in the mixing processes of the various simulations. We conclude that time-dependent transport patterns, especially between the Northern and the Southern Hemispheres, affect internal model variability significantly.

[47] **Acknowledgments.** We acknowledge support from the NASA Carbon Cycle Science and the NASA High-End Computing Program. This research used resources of the National Center for Computational Sciences at Oak Ridge National Laboratory (ORNL).

References

Andres, R. J., G. Marland, I. Fung, and E. Matthews (1996), A 1° × 1° distribution of carbon dioxide emissions from fossil fuel consumption and cement manufacture, 1950–1990, *Global Biogeochem. Cycles*, *10*, 419–429, doi:10.1029/96GB01523.

Baker, D. F., et al. (2006), TransCom 3 inversion intercomparison: Impact of transport model errors on the interannual variability of regional CO_2 fluxes, 1988–2003, *Global Biogeochem. Cycles*, *20*, GB1002, doi:10.1029/2004GB002439.

Bowman, K. P., and P. J. Cohen (1997), Interhemispheric exchange by seasonal modulation of the Hadley Circulation, *J. Atmos. Sci.*, *54*, 2045–2059, doi:10.1175/1520-0469(1997)054<2045:IEBSMO>2.0.CO;2.

Chou, M.-D., and M. J. Suarez (1999), A solar radiation parameterization for atmospheric studies, *NASA Tech. Rep.*, *104606*, vol. 15, 40 pp.

Chou, M.-D., M. J. Suarez, X. Z. Liang, and M. M.-H. Yan (2001), A thermal infrared radiation parameterization for atmospheric studies, *NASA Tech. Rep.*, *104606*, vol. 19, 56 pp.

Conway, T. J., P. P. Tans, L. S. Waterman, K. W. Thoning, D. R. Kitzis, K. A. Masarie, and N. Zhang (1994), Evidence for interannual variability of the carbon cycle from the National Oceanic and Atmospheric Administration/Climate Monitoring and Diagnostics Laboratory Global Air Sampling Network, *J. Geophys. Res.*, *99*(D11), 22,831–22,855, doi:10.1029/94JD01951.

Denning, A. S., P. J. Rayner, R. M. Law, and K. R. Gurney (1998), Atmospheric Tracer Transport Model Intercomparison Project (TransCom), *IGBP/GAIM Rep. 4*, NCAR, Boulder, Colo.

Denning, A. S., et al. (1999), Three-dimensional transport and concentration of SF6—A model intercomparison study (TransCom 2), *Tellus, Ser. B*, *51*, 266–297, doi:10.1034/j.1600-0889.1999.00012.x.

Erickson, D. J., III, P. J. Rasch, P. P. Tans, P. Friedlingstein, P. Ciais, E. Maier-Reimer, K. Kurz, C. A. Fischer, and S. Walters (1996), The seasonal cycle of atmospheric CO_2: A study based on the NCAR Community Climate Model (CCM2), *J. Geophys. Res.*, *101*, 15,079–15,097.

Erickson, D. J., III, R. T. Mills, J. Gregg, T. J. Blasing, F. M. Hoffman, R. J. Andres, M. Devries, Z. Zhu, and S. R. Kawa (2008), An estimate of monthly global emissions of anthropogenic CO_2: Impact on the seasonal cycle of atmospheric CO_2, *J. Geophys. Res.*, *113*, G01023, doi:10.1029/2007JG000435.

Gurney, K. R., et al. (2002), Towards robust regional estimates of CO_2 sources and sinks using atmospheric transport models, *Nature*, *415*, 626–630, doi:10.1038/415626a.

Gurney, K. R., Y.-H. Chen, T. Maki, S. R. Kawa, A. Andrews, and Z. Zhu (2005), Sensitivity of atmospheric CO_2 inversions to seasonal and interannual variations in fossil fuel emissions, *J. Geophys. Res.*, *110*, D10308, doi:10.1029/2004JD005373.

Heimann, M., and C. D. Keeling (1986), Meridional eddy diffusion model of the transport of atmospheric carbon dioxide: 1. Seasonal carbon cycle over the tropical Pacific Ocean, *J. Geophys. Res.*, *91*, 7765–7781, doi:10.1029/JD091iD07p07765.

Heimann, M., and M. Reichstein (2008), Terrestrial ecosystem carbon dynamics and climate feedbacks, *Nature*, *451*, 289–292, doi:10.1038/nature06591.

Kawa, S. R., D. J. Erickson III, S. Pawson, and Z. Zhu (2004), Global CO_2 transport simulations using meteorological data from the NASA data assimilation system, *J. Geophys. Res.*, *109*, D18312, doi:10.1029/2004JD004554.

Keeling, C. D., R. B. Bacastow, A. E. Bainbridge, C. A. Ekdahl, P. R. Guenther, and L. S. Waterman (1976), Atmospheric carbon dioxide variations at Mauna Loa Observatory, Hawaii, *Tellus*, *28*, 538–551, doi:10.1111/j.2153-3490.1976.tb00701.x.

Keeling, C. D., S. C. Piper, and M. Heimann (1989), A three-dimensional model of atmospheric CO_2 transport based on observed winds: 4. Mean annual gradients and interannual variations, in *Aspects of Climate Variability in the Pacific and the Western Americas*, *Geophys. Monogr. Ser.*, vol. 55, edited by D. H. Peterson, pp. 305–363, AGU, Washington, D. C., doi:10.1029/GM055p0305.

Kendall, W., J. Wang, M. Allen, T. Peterka, J. Huang, and D. Erickson (2011), Simplified parallel domain traversal, paper presented at SC '11: International Conference for High Performance Computing, Networking, Storage and Analysis, ACM, New York.

Law, R. M., et al. (1996), Variations in modeled atmospheric transport of carbon dioxide and the consequences for CO_2 inversions, *Global Biogeochem. Cycles*, *10*, 783–796, doi:10.1029/96GB01892.

Law, R. M., et al. (2003), TransCom 3 CO_2 inversion intercomparison: 2. Sensitivity of annual mean results to data choices, *Tellus. Ser. B*, *55*, 580–595.

Law, R. M., et al. (2008), TransCom model simulations of hourly atmospheric CO_2: Experimental overview and diurnal cycle results for 2002, *Global Biogeochem. Cycles*, *22*, GB3009, doi:10.1029/2007GB003050.

Lin, S.-J. (2004), A "vertically Lagrangian" finite-volume dynamical core for global models, *Mon. Weather Rev.*, *132*, 2293–2307, doi:10.1175/1520-0493(2004)132<2293:AVLFDC>2.0.CO;2.

Lock, A. P., A. R. Brown, M. R. Bush, G. M. Martin, and R. N. B. Smith (2000), A new boundary layer mixing scheme. Part I: Scheme description and single-column model tests, *Mon. Weather Rev.*, *128*, 3187–3199, doi:10.1175/1520-0493(2000)128<3187:ANBLMS>2.0.CO;2.

Louis, J., M. Tiedtke, and J. Geleyn (1982), A short history of the PBL parameterization at ECMWF, paper presented at Workshop on Planetary Boundary Layer Parameterization, ECMWF, Reading, U. K.

Masarie, K. A., et al. (2011), Impact of CO_2 measurement bias on CarbonTracker surface flux estimates, *J. Geophys. Res.*, *116*, D17305, doi:10.1029/2011JD016270.

Moorthi, S., and M. J. Suarez (1992), Relaxed Arakawa-Schubert: A parameterization of moist convection for general-circulation models, *Mon. Weather Rev.*, *120*, 978–1002, doi:10.1175/1520-0493(1992)120<0978:RASAPO>2.0.CO;2.

Olivier, J. G. J., and J. J. M. Berdowski (2001), Global emissions sources and sinks, in *The Climate System*, edited by J. Berdowski, R. Guicherit, and B. J. Heij, pp. 33–78, A.A. Balkema, Lisse, Netherlands.

Ott, L., B. Duncan, S. Pawson, P. Colarco, M. Chin, C. Randles, T. Diehl, and J. E. Nielsen (2010), Influence of the 2006 Indonesian biomass burning aerosols on tropical dynamics studied with the GEOS.5 AGCM, *J. Geophys. Res.*, *115*, D14121, doi:10.1029/2009JD013181.

Ott, L. E., S. Pawson, and J. T. Bacmeister (2011), An analysis of the impact of convective parameter sensitivity on simulated global atmospheric CO distributions, *J. Geophys. Res.*, *116*, D21310, doi:10.1029/2011JD016077.

Patra, P. K., et al. (2006), Sensitivity of inverse estimation of annual mean CO_2 sources and sinks to ocean-only sites versus all-sites observational networks, *Geophys. Res. Lett.*, *33*, L05814, doi:10.1029/2005GL025403.

Peters, W., et al. (2007), An atmospheric perspective on North American carbon dioxide exchange: CarbonTracker, *Proc. Natl. Acad. Sci. U. S. A.*, *104*(48), 18,925–18,930, doi:10.1073/pnas.0708986104.

Randerson, J. T., M. V. Thompson, T. J. Conway, I. Y. Fung, and C. B. Field (1997), The contribution of terrestrial sources and sinks to trends in the seasonal cycle of atmospheric carbon dioxide, *Global Biogeochem. Cycles*, *11*, 535–560, doi:10.1029/97GB02268.

Randerson, J. T., G. R. van der Werf, L. Giglio, G. J. Collatz, and P. S. Kasibhatla (2007), Global Fire Emissions Database, Version 2(GFEDv2.1), http://daac.ornl.gov/VEGETATION/guides/global_fire_emissions_v2.1.html, Oak Ridge Natl. Lab., Oak Ridge, Tenn., doi:10.3334/ORNLDAAC/849.

Rienecker, M. M., et al. (2008), The GEOS-5 Data Assimilation System—Documentation of versions 5.0.1, 5.1.0, and 5.2.0, *NASA Tech. Memo.*, *NASA/TM–2008–104606*, vol. 27, 118 pp.

Takahashi, T., R. H. Wanninkhof, R. A. Feely, and R. F. Weiss, D. W. Chipman, N. Bates, J. Olafsson, C. Sabine, and S. C. Sutherland (1999), Net sea–air CO_2 flux over the global oceans: An improved estimate based on the sea–air pCO_2 difference, in *Proceedings of the Second International Symposium: CO_2 in the Oceans*, edited by Y. Nojiri, pp. 9–14, Cent. for Global Environ. Res., Natl. Inst. for Environ. Stud., Tsukuba, Japan.

Tans, P. P., T. J. Conway, and T. Nakazawa (1989), Latitudinal distribution of the sources and sinks of atmospheric carbon dioxide derived from surface observations and an atmospheric transport model, *J. Geophys. Res.*, *94*(D4), 5151–5172, doi:10.1029/JD094iD04p05151.

van der Werf, G. R., J. T. Randerson, L. Giglio, G. J. Collatz, and P. S. Kasibhatla (2006), Interannual variability in global biomass burning emission from 1997 to 2004, *Atmos. Chem. Phys.*, *6*, 3423–3441, doi:10.5194/acp-6-3423-2006.

Young, W., A. Pumir, and Y. Pomeau (1989), Anomalous diffusion of tracer in convection rolls, *Phys. Fluids A*, *1*, 462–469, doi:10.1063/1.857415.